ARMY RESEARCH LABORATORY

Time-Frequency Analysis of a Moving Human Doppler Signature

by Traian Dogaru, Calvin Le, and Getachew Kirose

ARL-TR-4728 **February 2009**

NOTICES

Disclaimers

The findings in this report are not to be construed as an official Department of the Army position unless so designated by other authorized documents.

Citation of manufacturer's or trade names does not constitute an official endorsement or approval of the use thereof.

Destroy this report when it is no longer needed. Do not return it to the originator.

Army Research Laboratory
Adelphi, MD 20783-1197

ARL-TR-4728 **February 2009**

Time-Frequency Analysis of a Moving Human Doppler Signature

Traian Dogaru, Calvin Le, and Getachew Kirose
Sensors and Electron Devices Directorate, ARL

REPORT DOCUMENTATION PAGE

Form Approved
OMB No. 0704-0188

1. REPORT DATE *(DD-MM-YYYY)*	2. REPORT TYPE	3. DATES COVERED (From - To)
February 2009	Final	2007 to 2008

4. TITLE AND SUBTITLE
Time-Frequency Analysis of a Moving Human Doppler Signature

5a. CONTRACT NUMBER

5b. GRANT NUMBER

5c. PROGRAM ELEMENT NUMBER

6. AUTHOR(S)
Traian Dogaru, Calvin Le, and Getachew Kirose

5d. PROJECT NUMBER

5e. TASK NUMBER

5f. WORK UNIT NUMBER

7. PERFORMING ORGANIZATION NAME(S) AND ADDRESS(ES)
U.S. Army Research Laboratory
ATTN: AMSRD-ARL-SE-RU
2800 Powder Mill Road
Adelphi, MD 20783-1197

8. PERFORMING ORGANIZATION REPORT NUMBER
ARL-TR-4728

9. SPONSORING/MONITORING AGENCY NAME(S) AND ADDRESS(ES)

10. SPONSOR/MONITOR'S ACRONYM(S)

11. SPONSOR/MONITOR'S REPORT NUMBER(S)

12. DISTRIBUTION/AVAILABILITY STATEMENT
Approved for public release; distribution unlimited.

13. SUPPLEMENTARY NOTES

14. ABSTRACT
In this report we analyze the Doppler signature of a moving human with the purpose of finding temporal change patterns that would allow detection and classification of movers. The analysis is based on computer models that simulate the operation of a pulse-Doppler radar. We start with an animated human mesh in walking motion and compute the frame-by-frame radar return using electromagnetic solvers such as the Finite Difference Time Domain (FDTD). The results are processed in the time-frequency domain via Short-Time Fourier Transforms (STFT) and displayed as spectrograms. In the end, we try to distinguish patterns in these spectrograms that are characteristic to a certain human motion type. The analysis emphasizes the phenomenological aspects of the Doppler signature, by looking at the relative contribution of various body parts and the effect of frequency, aspect angle, polarization and other radar parameters.

15. SUBJECT TERMS
Doppler radar, time-frequency analysis

16. SECURITY CLASSIFICATION OF:			17. LIMITATION OF ABSTRACT	18. NUMBER OF PAGES	19a. NAME OF RESPONSIBLE PERSON
a. REPORT	b. ABSTRACT	c. THIS PAGE	UU	34	Traian Dogaru
U	U	U			19b. TELEPHONE NUMBER (*Include area code*) 301-394-1482

Standard Form 298 (Rev. 8/98)
Prescribed by ANSI Std. Z39.18

Contents

List of Figures

Acknowledgments

This study was partially funded by the Communications-Electronics Research Development and Engineering Center (CERDEC), Intelligence and Information Warfare Directorate (I2WD) at Ft. Monmouth, NJ, and the Office of Naval Research (ONR) in Arlington, VA.

1. Introduction

The U.S. Army has shown great interest in the problem of radar detection and classification of moving humans, dating back to the Vietnam War era. Using the Doppler spectrum of the radar response may offer the only solution for detecting moving targets concealed behind obstacles, such as vegetation or building structures. The interest in this technology has been recently renewed by large-scale research and development efforts conducted by defense agencies in sensing through the wall (STTW) and foliage penetration (FOPEN) radar sensors. The major challenge with this approach is that any moving objects (such as blowing leaves, household appliances, etc.) or animals present in the scene can produce a Doppler response, thereby creating false alarms. In order to reliably discriminate human movers from other types of movers, we need to perform a more complex analysis of the Doppler signature and extract features characteristic to a certain target. Moreover, such analysis may enable us to extract biometric features of a person (for instance, tall vs. short person, or weapon-carrier vs. non-weapon-carrier). The research work described in this report represents an effort in this direction.

Over the last decade, the Radio Frequency (RF) Signal Processing and Modeling Branch at the U.S. Army Research Laboratory (ARL) has made a significant investment in both electromagnetic modeling tools as well as wideband radar measurement instruments. We have applied both of these to the problem of detecting humans concealed behind obstacles. ARL is currently involved in three major defense programs related to sensing through the wall and foliage penetration radar, where the moving human detection and recognition problem is a key component.

In some preliminary work (*1*–*3*) we have thoroughly analyzed the radar signature of humans in static configurations, for various positions and radar parameters, based on computer simulations. We started with realistic body meshes, and used sophisticated mesh manipulation and conversion software packages in order to reconfigure the body in various positions. For the electromagnetic (EM) scattering analysis we employed software tools such as Xpatch (a ray-tracing code) and the Finite-Difference Time-Domain (FDTD). These studies provided us with a wealth of information on the human radar cross-section variability with regard to body type, position, aspect angle and frequency.

The next step consists of analyzing the radar response from a moving human, with the hope to extract certain features that allow classification of humans versus other movers. This problem has received an early interest within the defense research community, as demonstrated by work done at the Harry Diamond Laboratories (now ARL) in the 1970s (*4*). The initial approach consisted of using the stationary Doppler spectrum of various movers for classification purposes. More recently, researchers started focusing on understanding the temporal changes in the Doppler spectrum via time-frequency analysis techniques (*5*–*8*). Most of the work published so

far in the literature is based on simplistic computer models of a moving human. On the other hand, our research group at ARL has developed the unique capability to combine powerful software tools and hardware platforms in order to tackle this problem in realistic detail. In this report, we outline the methodology involved in the time-frequency analysis of the human Doppler signature, based on computer models. We particularly emphasize the effect of radar system parameters as they relate to the EM scattering phenomenology.

This report is organized as follows. In section 2 we present the computational tools and describe the methodology involved in this analysis. In section 3 we show the results obtained for a walking human in various configurations, in different frequency bands and at several aspect angles. We finalize with conclusions in section 4.

2. Methodology

The time-frequency analysis of the moving human Doppler signature presented in this section is based entirely on computer models. In essence, we are simulating the operation of a pulse-Doppler radar (*9*), where the responses from successive transmitted pulses are processed together in order to extract the Doppler frequency shift. In our computer models, the moving target is frozen in time for the duration of each pulse. Thus, we need to decompose the human motion into frames that succeed each other with the radar's pulse repetition frequency (PRF). Then we use an EM solver to compute the radar return for a given excitation pulse, for each frame.

The basic equation that links the Doppler frequency shift to the target velocity is:

$$f_D = \frac{2v}{c} f_c \tag{1}$$

where f_D is the Doppler shift, f_c is the center pulse frequency, v is the target velocity and c is the speed of light. This equation shows that a larger radar center frequency results in a larger Doppler shift (thus, the radar is more sensitive to moving targets). However, since our applications involve penetrating lossy materials (such as walls or vegetation), we are constrained to operate at relatively low frequencies (typically around 1 GHz for STTW radar and 300 MHz for FOPEN radar).

We start the computer modeling with the triangular facet mesh of the "fit man" in the basic standing position. This mesh was introduced in (*1*). It describes only the outer shell of the human body, so we must assume that the body is made of a uniform dielectric material. We picked $\varepsilon_r = 50$ and $\sigma = 1$ S/m for the body material, which are close to the skin dielectric properties. In references (*1,3*) we compared the uniform dielectric model of a human body with the full model (where each different tissue is assigned the actual permittivity) and concluded that both models produce very similar radar cross section (RCS) in the frequency bands of interest.

In this study we place the human body in the open space (i.e., not behind walls or other obstacles). That means, when the depression angle is 0°, the background medium is free-space, whereas for positive depression angles we consider a half-space background (as in section 3.6).

A software package named Maya (produced by Autodesk, Inc. [*10*]) allowed us to articulate this mesh in various body positions. Moreover, Maya can create realistic animation of a human in motion by interpolating the mesh in an arbitrary number of frames between only a few reference positions. In figure 1 we represented several frames of the walking human mesh obtained with Maya. In our study, we assumed that each complete walking cycle (two strides per cycle) takes 2 seconds, and the average velocity is about 0.6 m/s. The PRF (or number of frames per second) must be high enough in order to avoid aliasing in the Doppler domain (*9*) at the highest radar operational frequency considered in this study. Thus, the maximum target velocity that can be unambiguously captured by the radar is:

$$v_{\max} = \frac{c}{4}\frac{PRF}{f_c} \tag{2}$$

In our simulations we used a total of 80 frames, which implies a *PRF* of 40 Hz. That results in $v_{\max}$ = 3 m/s for f_c = 1 GHz, which is more than any body part can generate during the walking motion.

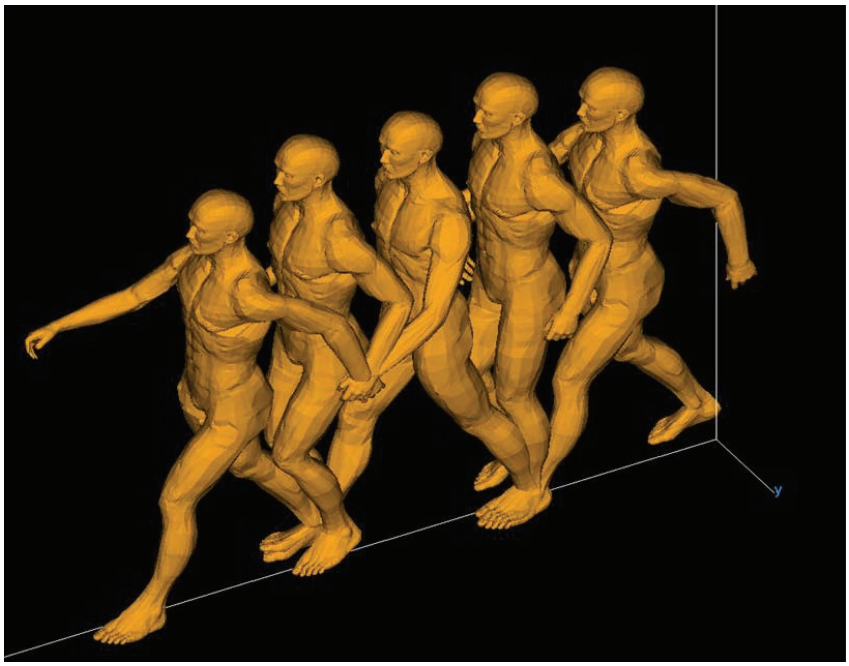

Figure 1. Successive frames of the fit man mesh in walking motion, created by the Maya software package.

The radar signature of each frame is computed using AFDTD. This is a computational electromagnetic (CEM) code entirely developed at ARL for radar signature calculations. It is

based on the Finite Difference Time Domain (FDTD) technique, which has been described in other reports (*1–3*). An excellent introduction to the FDTD method can be found in textbooks such as (*11,12*). We emphasize that calculating the human body signature at the relatively low frequencies considered in this report (from 300 MHz to 1GHz) requires a full-wave CEM method (such as FDTD), since approximate methods (such as those based on ray tracing) may not produce results accurate enough for these scenarios. The FDTD meshes that we used in these simulations have a resolution (cell size) of 5 mm, which is sufficient for frequencies up to 1 GHz (for more details see [*1*]). We also need to mention that all the calculations in this report are performed in the far-field, and involve plane-wave excitation at a given set of incidence angles.

For the Doppler analysis in this study we use relatively narrowband excitation pulses (with bandwidth between 40 and 80 MHz). The EM scattering data is obtained in the frequency domain and the pulse is synthesized back to the time domain by using an appropriate frequency window. We designed this frequency window such that the time domain pulse envelope that we obtain through inverse Fourier transform has a shape as close to rectangular as possible. We sample the returned narrowband pulse corresponding to each frame in order to obtain the in-phase (I) channel data (all the pulses need to be sampled at the same moment in time relative to a fixed reference). We also obtain the quadrature (Q) channel data by sampling the Hilbert transform (*13*) of the returned narrowband pulse described above. One requirement for this type of analysis is that the entire walking cycle be contained inside one down-range bin, such that the sampling instant "catches" some part of each pulse received during the cycle. This puts an upper limit on the excitation pulse bandwidth. Also notice that a narrower bandwidth implies lower down-range resolution, therefore, the target is less localized. The relationship between the down-range bin size and the bandwidth is:

$$\Delta R = \frac{c}{2BW} \tag{3}$$

where BW is the bandwidth and ΔR is the down-range resolution (or bin size). Since the human covers about 1.2 m during a walking cycle, the maximum pulse bandwidth allowed is 125 MHz.

The I-Q data is used in extracting the Doppler frequency shift information by taking Fourier transforms. Since we are interested in the time variation of the Doppler spectrum, we employ short-time Fourier transforms (STFT) (*13*) that use only part of the I-Q data sequence at a time. The length of the time window in the STFT is called the coherent processing interval (CPI), or dwell time, and is typically just a fraction of a walking cycle period. Since we use a Hanning window (*13*) in the time domain, the effective CPI (which is the value listed for each of the cases considered in this report) is half the time interval between the zero-crossing points of the window. A large CPI implies good frequency resolution in the Doppler spectrum, but poor resolution in the time domain, so a compromise between the two must be achieved. The relationship between the frequency resolution Δf and the time resolution (effective CPI) is:

$$\Delta f = \frac{1}{CPI} \tag{4}$$

We use the maximum possible overlap between the time-domain windows by setting the shift between two successive windows at only one slow time sample. Since we consider the walking motion as cyclical, we can wrap around the I-Q sequence corresponding to one cycle into an infinite loop, thus making sure that there are no spurious jumps in the STFT data at the beginning and end of the cycle.

The sequence of STFTs is arranged in a matrix format (with slow time variation by rows and frequency variation by columns) and the magnitude is plotted as a two-dimensional pseudo-color map (in dB scale), also known as spectrogram. The abscissa represents the slow time, whereas the ordinate represents the velocity (which is proportional to the Doppler frequency shift). One spectrogram represents four walking cycles, in which the data generated by the first cycle is simply repeated another three times. This allows a better visualization of the patterns characteristic to human walking. The entire process described in this section is illustrated in figure 2. All the electromagnetic modeling of radar signatures was run on high-performance computing (HPC) platforms at the ARL Major Shared Resource Center (MSRC) (*14*), while desktop personal computers (PC) were used for processing the meshes and creating the spectrograms. The signal processing routines were implemented in MATLAB.

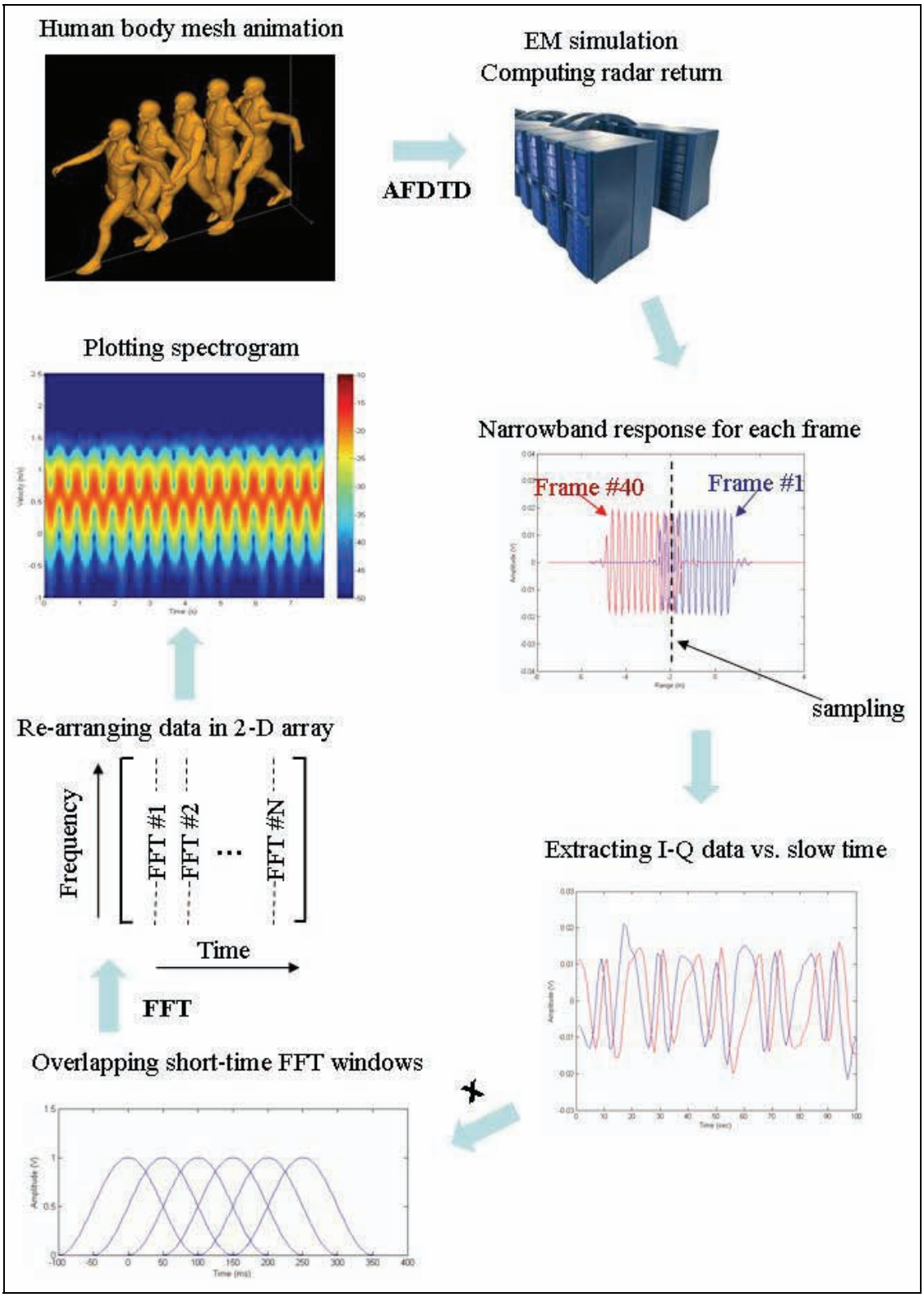

Figure 2. Schematic diagram showing the steps involved in obtaining Doppler spectrograms of a walking human based on computer models.

3. Numerical Results

3.1 Spectrograms of Regular Walking Motion at 1 GHz

In the following examples, unless otherwise specified, we consider that the human is facing and walking straight toward the radar. Since our EM modeling involves far-field geometries and plane-wave incidence, this translates to incidence at 0° azimuth and 0° elevation (as measured from the *x*-*y* plane). We consider vertical-vertical (V-V) polarization in most cases (unless otherwise specified). We start by analyzing the Doppler spectrograms obtained with the radar operating around 1 GHz, which is a good frequency band choice for STTW applications. In this particular case, the pulse bandwidth is 80 MHz and CPI is 0.3 seconds. The spectrogram is shown in figure 3.

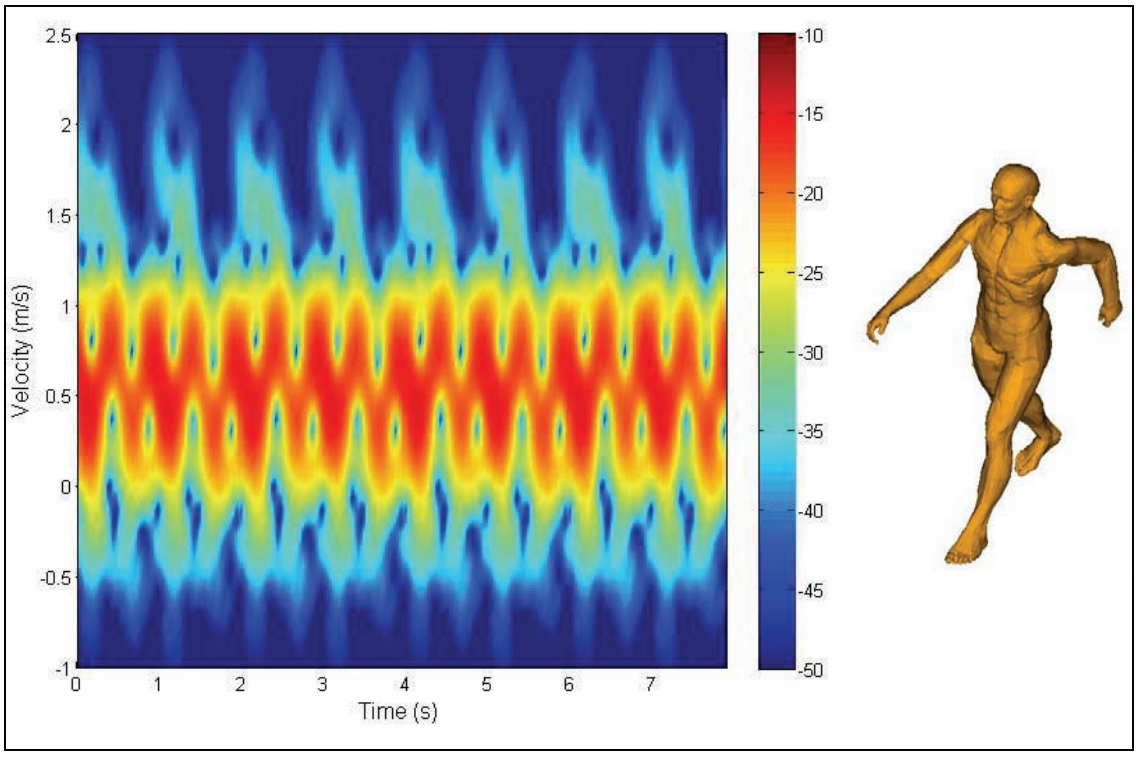

Figure 3. Spectrogram of the full human body in walking motion (directly towards the radar) at 1 GHz.

The most striking pattern that we notice in the spectrogram in figure 3 is the zigzag formed by the high-intensity (red) feature in the middle of the diagram. It is easy to prove that this feature closely follows the velocity of a point on the human's chest. Thus, in figure 4, we overlaid a thin black line representing the velocity of the point marked on the human's chest (as obtained directly from the mesh files). The important conclusion is that the velocity of the human's torso is not constant during walking, but it accelerates and decelerates according to the pattern visible in figure 4. If we draw a line through the middle of this pattern, we obtain the average velocity,

which is about 0.6 m/s. As we will show in the following section, the main contribution to the radar return (at these angles and frequencies), which creates the highest intensity feature in the spectrogram, comes from the human's torso. The lower intensity "spikes" (high velocity features) that we notice at the upper edge of the spectrogram represent the arms and legs contribution. As expected, there are instances when their velocity is higher than that of the torso, but the radar return is generally weaker. We should also mention that the features in the spectrogram display a certain amount of smearing, due to the limited resolution, both in time and frequency (velocity) domains.

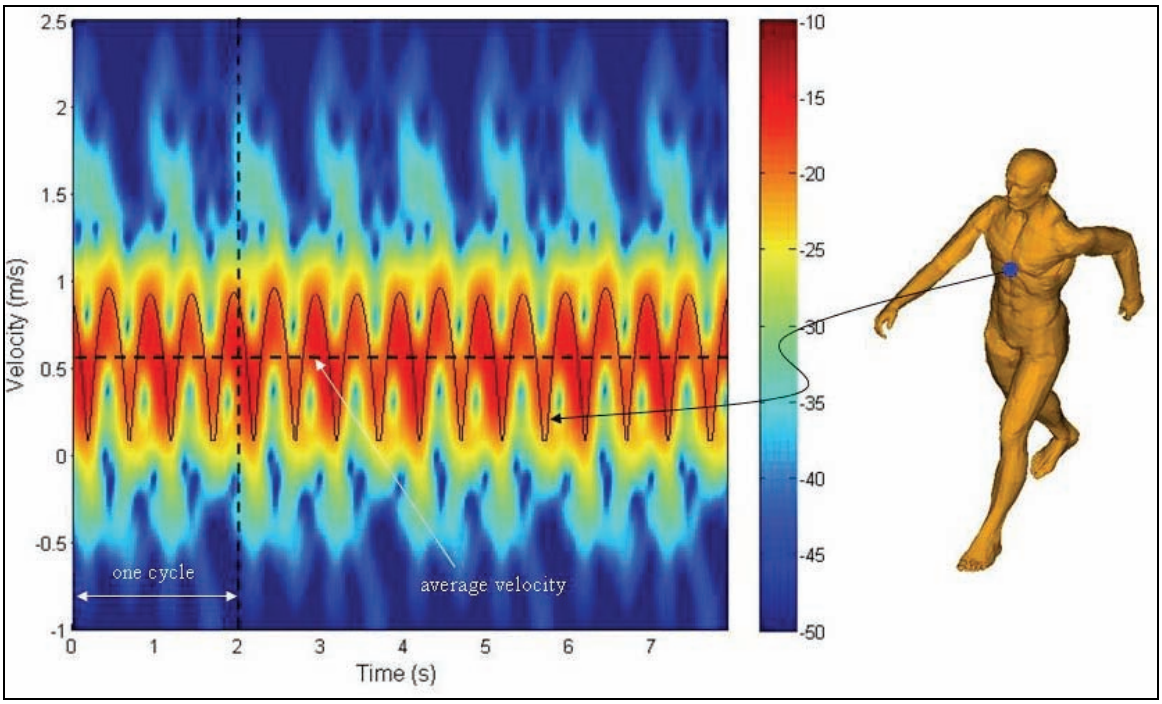

Figure 4. Spectrogram of the full human body in walking motion at 1 GHz, showing various walking cycle parameters, as well as the velocity of a point on the human's chest.

It is interesting to notice that the zigzag pattern visible in figures 3 and 4 is not necessarily unique to the walking motion of a human. In fact, any object that moves back and forth in an oscillatory type of motion (such as a pendulum) would create a similar zigzag pattern in the Doppler spectrogram. However, what is characteristic to the human walking motion is that all the velocities within the zigzag line are positive, meaning that the body is advancing in the forward direction, with non-uniform velocity (as opposed to an object that oscillates back and forth about an equilibrium position, where both positive and negative velocities would be generated).

3.2 Separating the Body Part Contributions to the Spectrogram at 1 GHz

In order to analyze the contribution of the various body parts to the spectrogram obtained in figure 3, we computed the radar signature of separate parts of the human body, frame by frame.

In figure 5 we show the spectrogram based on the head and torso alone (the radar parameters are the same as in section 3.1, and the mesh points move exactly the same as in that case). One can notice that the spectrograms in figures 3 and 5 look very similar, even in terms of magnitude (on the color scale). However, the high-velocity spikes in figure 3 are not present in figure 5, which demonstrates that they were produced by the arms and legs motion. It is interesting to notice that the spectrogram in figure 5 extends to negative velocities, despite the fact that all points in the partial torso-and-head mesh move strictly forward (so they have positive velocities). This is again the effect of frequency domain smearing due to the finite length STFTs and mentioned in the previous section.

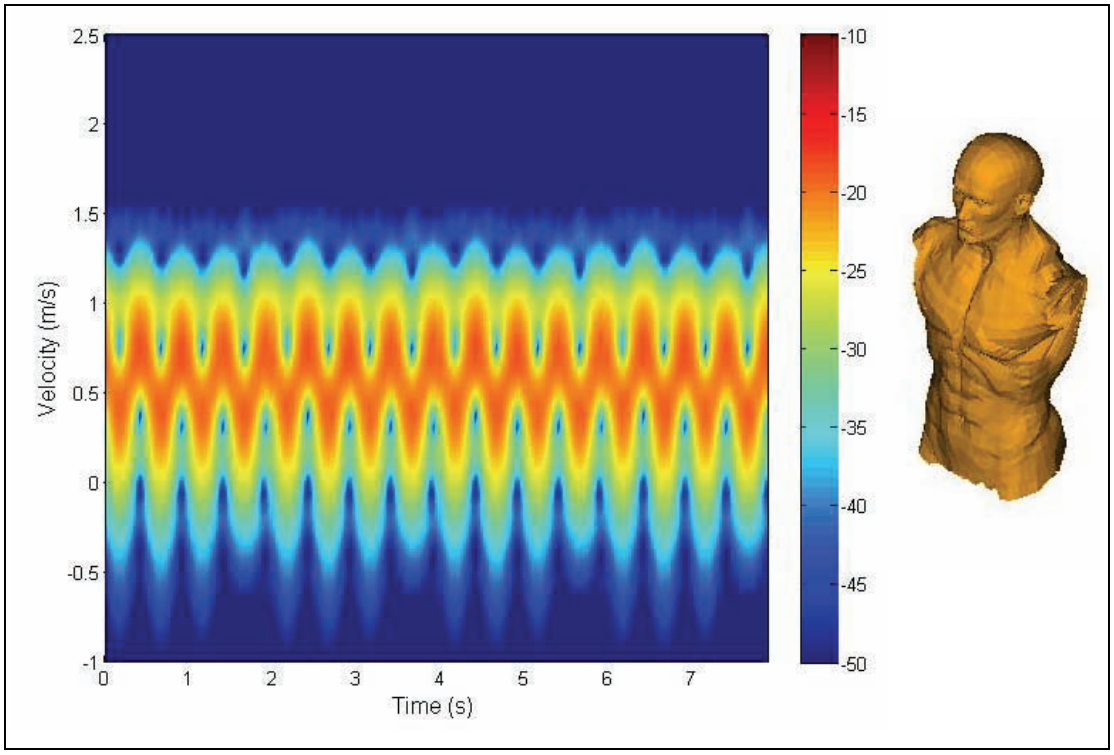

Figure 5. Spectrogram of the torso and head contribution to the Doppler signature at 1 GHz.

When we consider the arms and legs alone, we obtain the spectrogram in figure 6. We notice that the overall return is much weaker, but there are instances in the walking cycle when the velocity is much higher than that of the torso. Furthermore, we can separate the arm (figure 7) and leg contributions (figure 8). These spectrograms clearly demonstrate that the highest velocity components come from the arm motion. Both the legs and the arms seem to generate negative velocities in our model. At this point in our investigation, it is still unclear whether this feature is a realistic model for natural human walking.

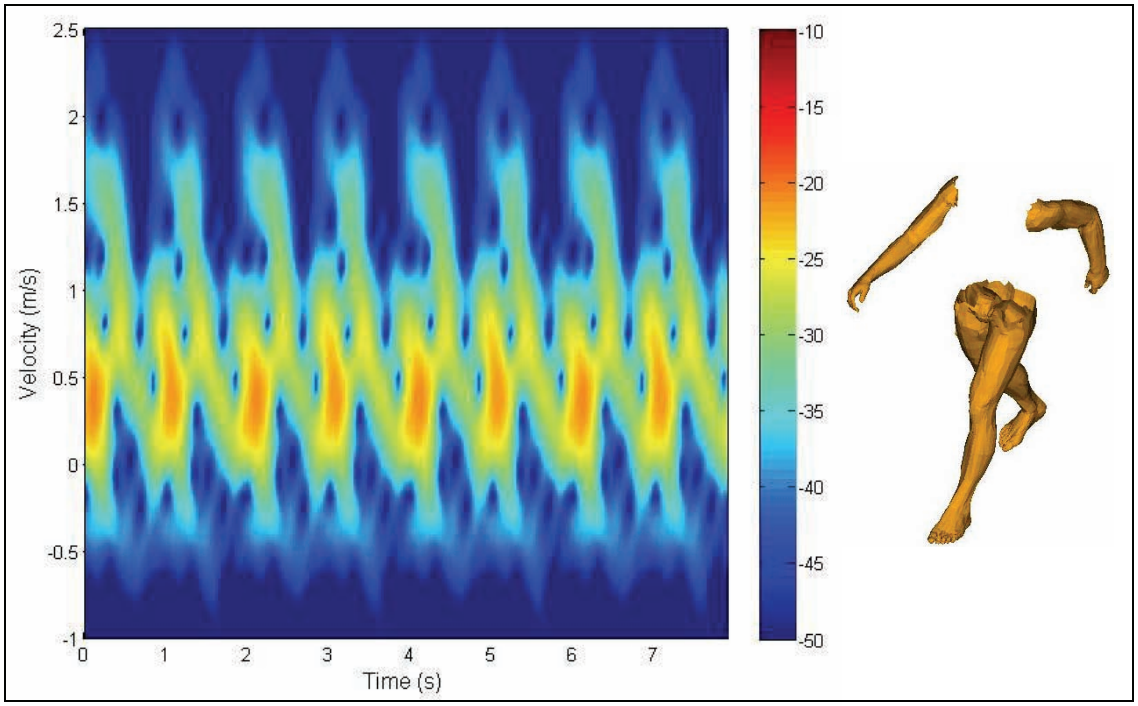

Figure 6. Spectrogram of the arms and legs contribution to the Doppler signature at 1 GHz.

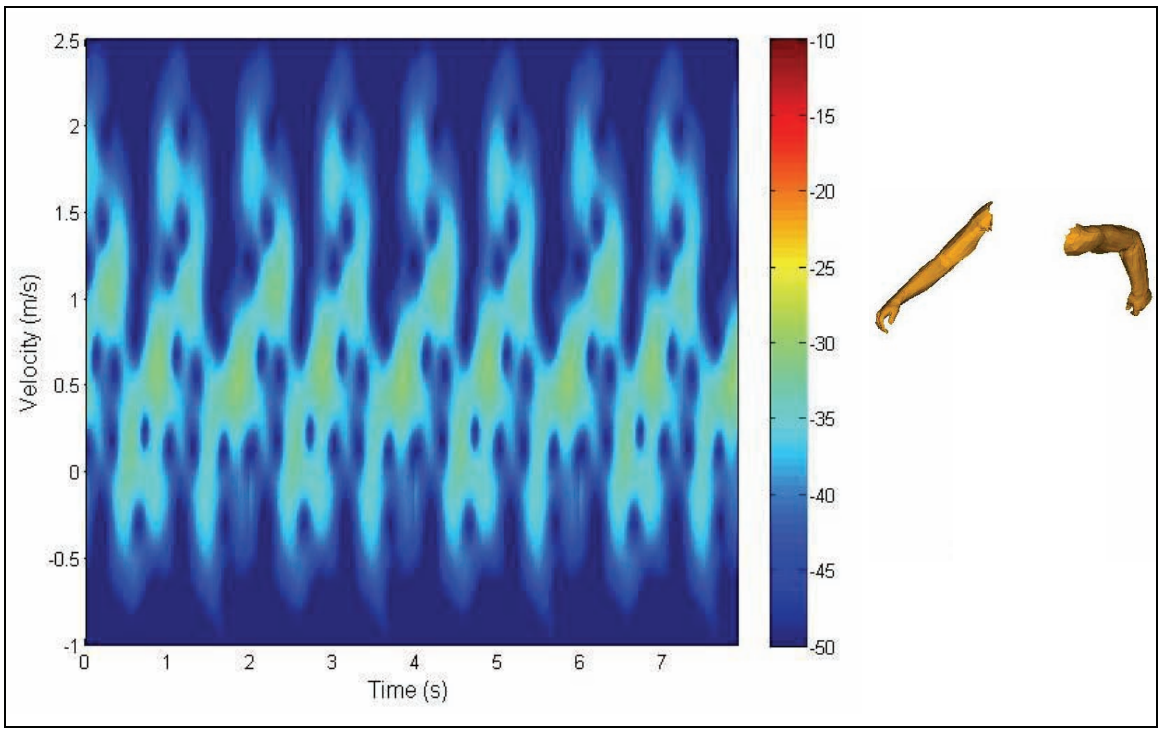

Figure 7. Spectrogram of the arms contribution to the Doppler signature at 1 GHz.

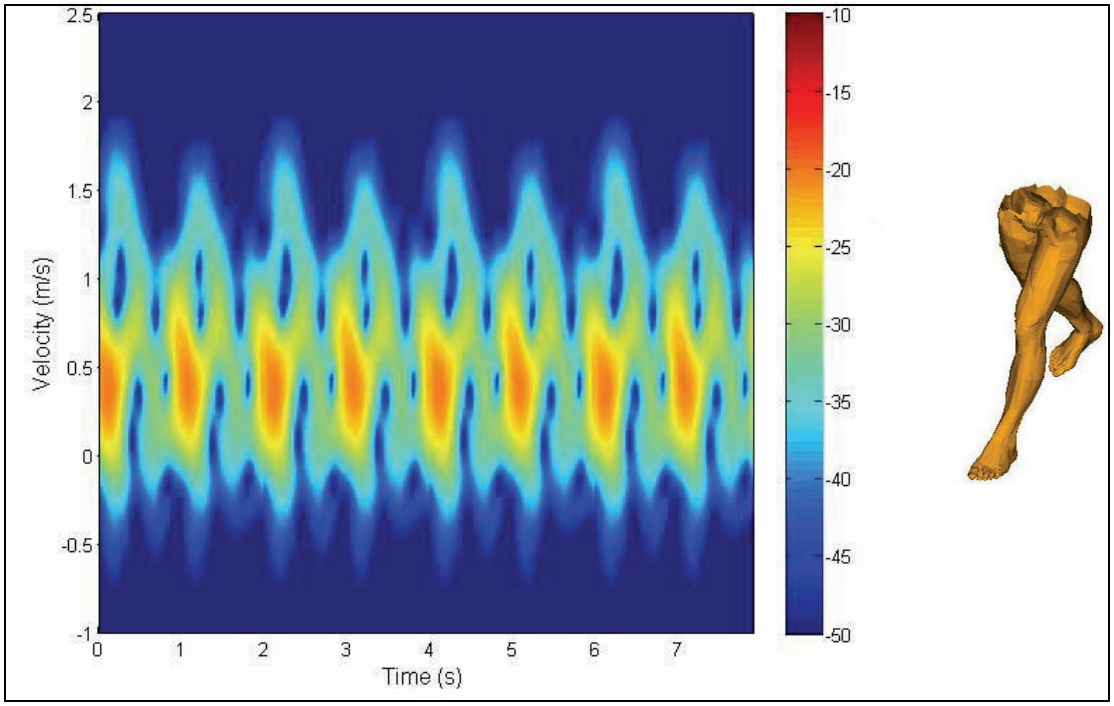

Figure 8. Spectrogram of the legs contribution to the Doppler signature at 1 GHz.

We also looked at the relative intensity of the radar return from various body parts during a walking cycle. In figure 9 we plot the RCS of the torso (including the head), the legs and the arms versus the frame number. As expected, the torso RCS is basically constant, since that part of the body does not change its orientation relative to the radar. However, the legs and arms display large variations in RCS, according to their orientation during a walking cycle. In particular, there are two leg positions that generate large RCS values, which can be seen both in figure 9, as well as in the spectrogram in figure 8 (the high-intensity spots of about –22 dB). For completeness, we also plotted the RCS of the legs and arms together (red line in figure 9). The fact that this line mostly follows the legs RCS (dominant between arms and legs), shows that there is not much coupling between the body parts at this radar frequency. Figure 10 captures the meshes (arms and legs only) corresponding to the frames where the legs contribution to the radar return peaks out. As we expect, the leg position in those frames is almost vertical, generating a relatively strong backscatter “flash”.

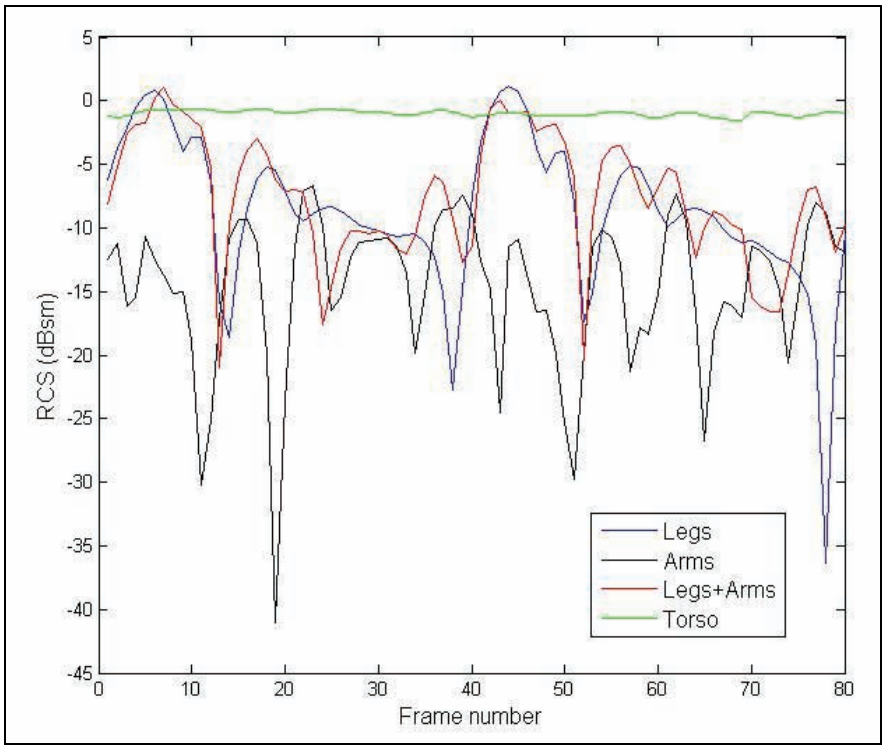

Figure 9. Frame-by-frame contribution of different body parts to the radar cross section at 1 GHz.

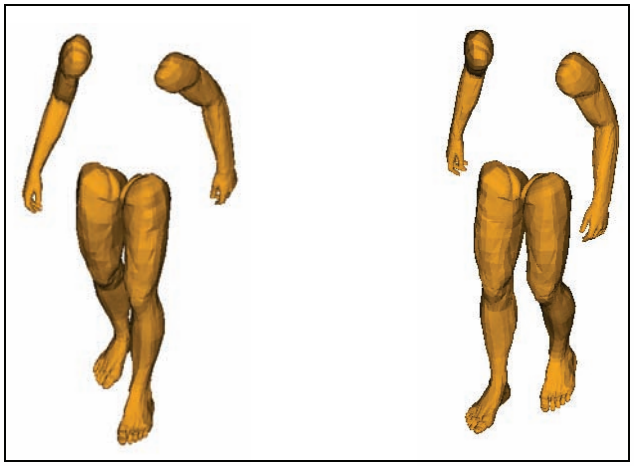

Figure 10. Arm and leg position for frames # 5 (left) and 45 (right), where the radar cross section peaks out at 1 GHz.

3.3 Spectrograms of a Walking Human Carrying an AK47 Rifle

One scenario of great interest is trying to classify a person carrying a weapon. In this section we consider the fit man carrying an AK47 in the port-arms position, as shown in figure 11. The human mesh displays the same walking pattern as in the previous sections, with the exception that the arms are in fixed position, holding the rifle. The AK47 mesh is based on a real-life

computer-aided design (CAD) model and contains parts made out of perfect electric conductor (PEC) and wood. The spectrogram obtained for this configuration is shown in figure 11 (all the radar parameters are identical to those in section 3.1). The first thing to notice is that the Doppler pattern is very similar to that of a human walking without the weapon. More precisely, there is a high degree of similarity with the spectrogram in figure 5, where only the torso and the head were considered. In both cases, the high velocity contribution of the swinging arms is absent. This suggests a quick way to infer whether the human target is suspect of carrying a weapon (for instance, by comparing the high velocity component intensity to the maximum intensity component of the spectrogram). However, one should keep in mind that a human who does not swing his/her arms is not always indicative for somebody carrying a weapon (it could also indicate for instance a person walking with his/her hands in the pockets).

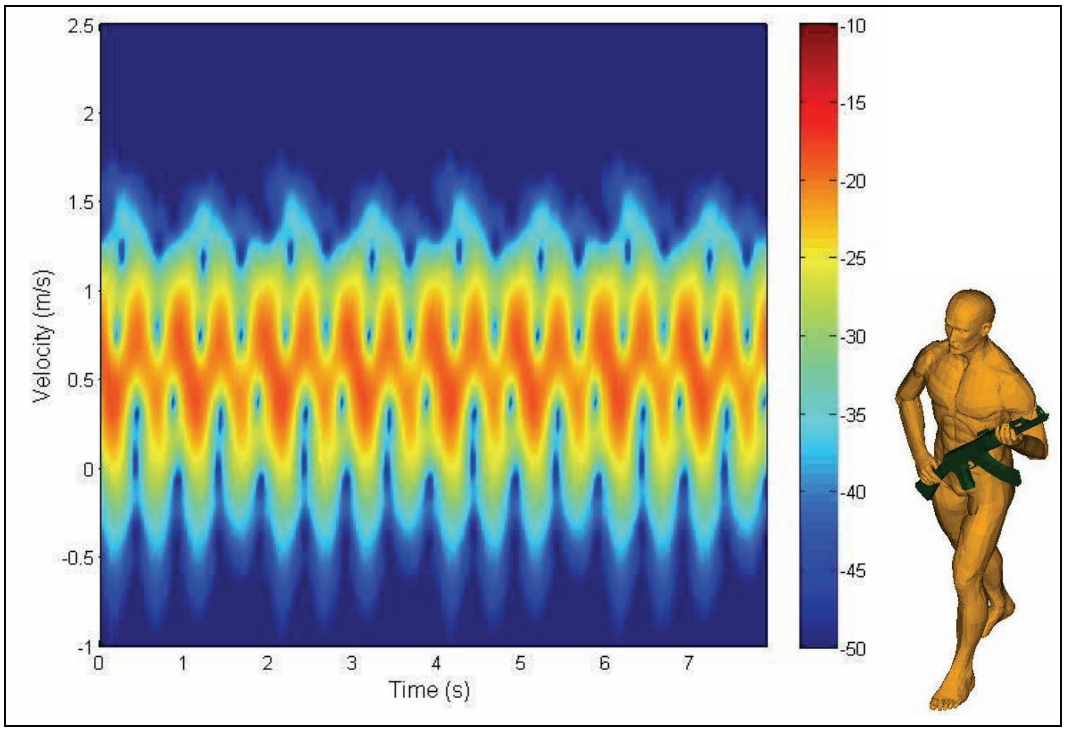

Figure 11. Spectrogram of the full human body in walking motion, carrying an AK47 rifle, at 1 GHz.

Another interesting thing to notice about the spectrogram in figure 11 is that, when a weapon is positioned in front of the human chest, the radar return decreases slightly as compared to the no weapon case. The explanation is that, for straight-on incidence, the rifle perturbs the "flat-plate" appearance of the chest, creating a return which is partially out-of-phase with the return from the chest and therefore, reducing the overall backscatter signal strength. This finding emphasizes the fact that trying to detect a weapon based on the magnitude of the radar signature alone is an unreliable method. Most likely, a fully polarimetric analysis of the radar scattering would significantly increase the chances of detecting the presence of a rifle-like object, whose signature is highly dependent of the polarization angle of the incident wave.

3.4 Comparison with Measurements

Although measurements that would allow us to compare the simulated Doppler spectrograms with direct radar data in the same frequency band were not available to us, we compared our results with Doppler spectrograms obtained experimentally by another ARL research group in the Ka radar band. (We mention here that performing these computer models in the Ka-band as opposed to the L-band would be very difficult because we would need a much higher *PRF*, which translates in a much larger number of frames within one walking cycle). The simulated and experimental spectrograms are shown side-by-side in figure 12 (the vertical scale was stretched in figure 12a as compared to the previous spectrograms). Notice that in the measurements the walking cycle is shorter than 2 s. Also, we do not have complete information about the vertical axis scale (other than the numbers represent Doppler bins), and the decibels scale or dynamic range of the pseudo-color map in figure 12b. However, despite all these limitations, we notice a good resemblance between the patterns in figures 12a and 12b. The zigzagging red line in the middle mainly represents the torso's contribution, whereas the spikes in the upper part of the diagrams represent the arms and legs contributions.

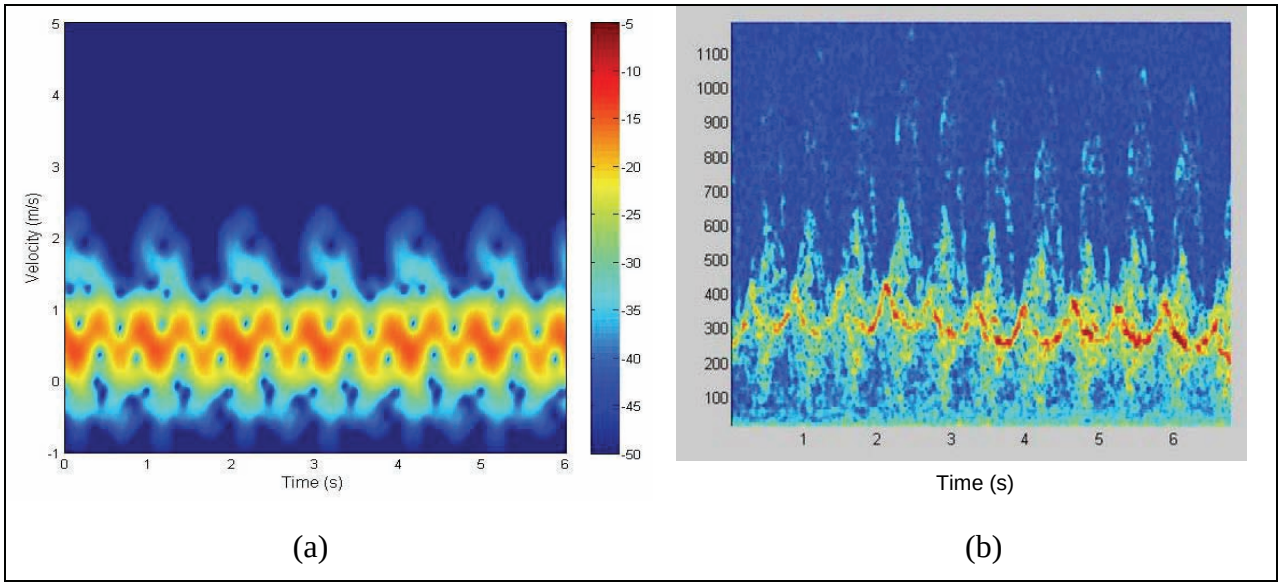

Figure 12. Comparison between simulated and measured Doppler spectrograms of a walking human, showing (a) simulated spectrogram at 1 GHz, and (b) measured spectrogram in the Ka-band.

3.5 Oblique Angle Incidence

All the spectrograms presented so far assume that the human is walking straight to the radar and the azimuth incidence angle is $\phi = 0°$. If we change the angle of incidence with respect to the walking direction, the radial velocity (which creates the Doppler frequency shift) decreases as $\cos\phi$ (9). Therefore, the amplitude of velocity oscillations in the spectrogram is smaller. In this section we keep the elevation angle at 0° and assume free-space propagation. All the radar parameters are identical to the previous sections, including the 1 GHz radar frequency.

The overall zigzag pattern that we mentioned in section 3.1 is distorted when the radar looks at an oblique angle. This is partially due to the fact that various body positions during the two half cycles are not symmetric from the radar point of view any longer. Figure 13 shows the spectrogram obtained for $\phi = 30°$, whereas figure 14 shows the case when $\phi = 60°$. We notice that the zigzag pattern distortion becomes more pronounced as the incidence angle increases. Also, as shown in figure 13, the arm contribution (high velocity "spikes") becomes stronger for one half of the cycle. One obvious explanation for the asymmetry is the fact that the arm placed further from the radar becomes shadowed (by the rest of the body) during half of the cycle and does not contribute to the overall radar return at that time. Similar to the analysis in section 3.2, we investigated the frame-by-frame RCS during a walking cycle, and found that, for $\phi = 60°$, the maximum response is achieved by frames #3 and 43 (which are also consistent with the brightest spots in the spectrogram in figure 14). We represented the human mesh positions for those two frames in figure 15. We conjecture that, in this case, the coupling between various body parts is more important than for straight-on incidence, in the sense that, for certain positions, the torso, arms and legs may form corners that enhance the radar return at specific incidence angles.

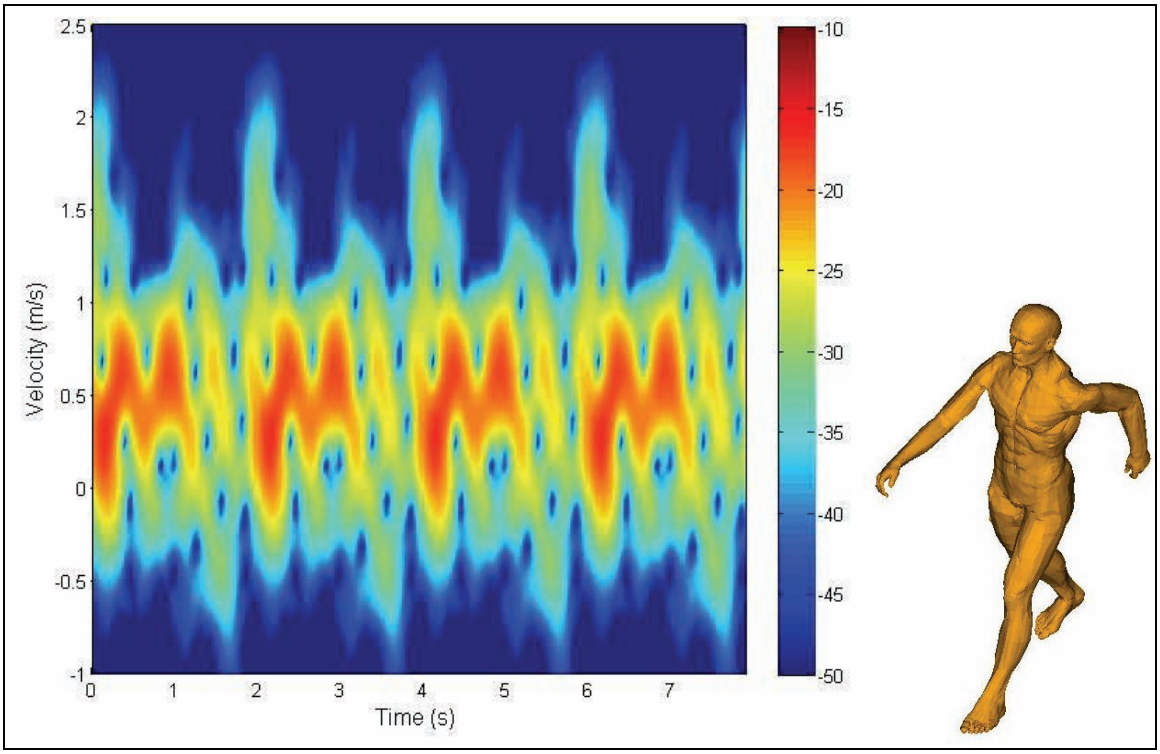

Figure 13. Spectrogram of the full human body in walking motion at 1 GHz, for a 30° azimuth incidence angle.

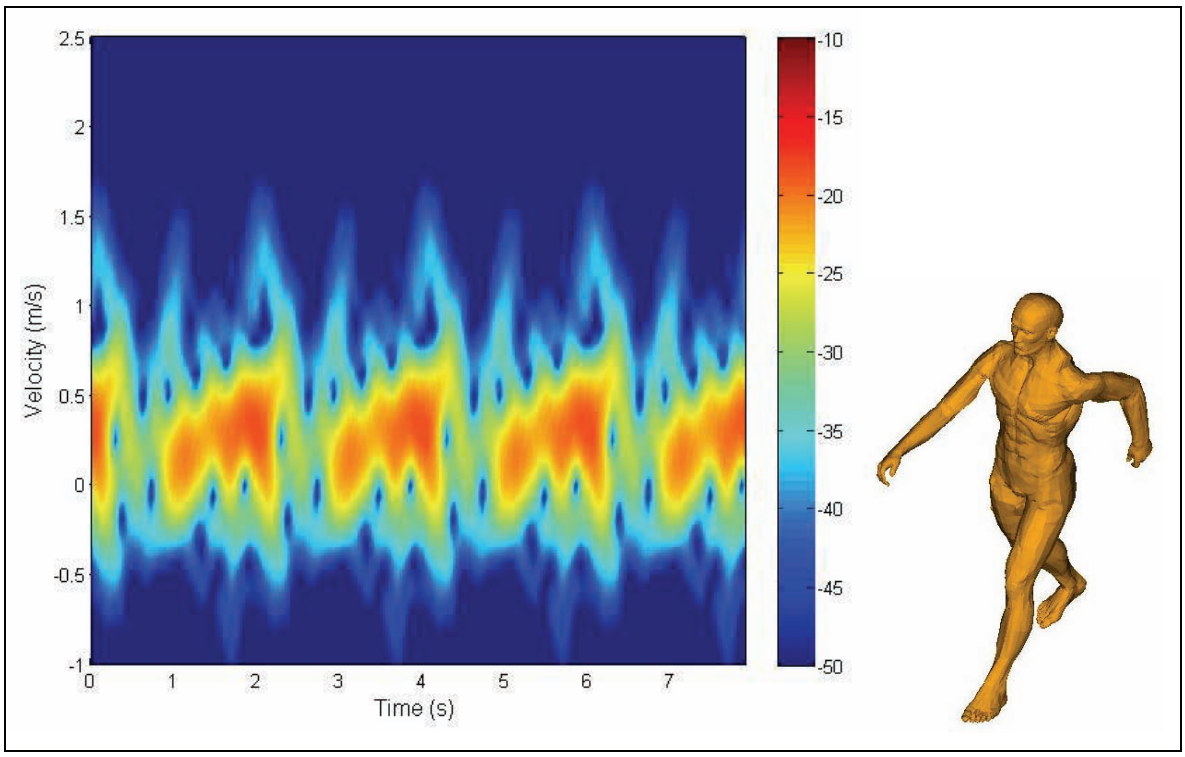

Figure 14. Spectrogram of the full human body in walking motion at 1 GHz, for a 60° azimuth incidence angle.

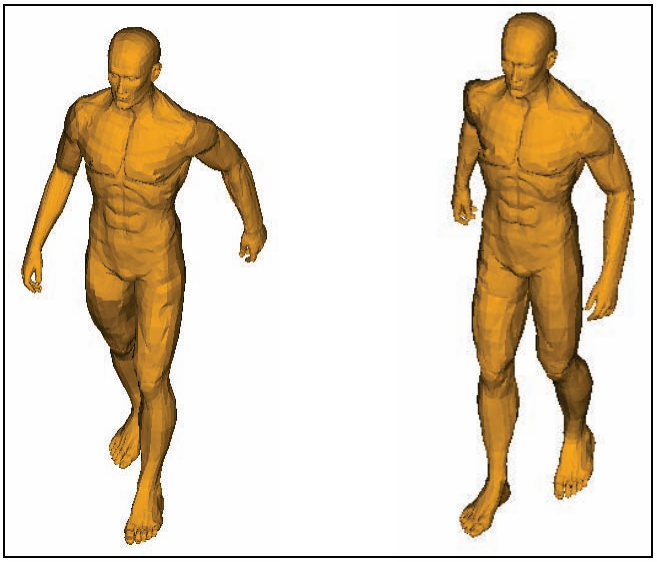

Figure 15. Views of the fit man body mesh corresponding to frames #3 (left) and 43 (right).

Another interesting feature that we see in the spectrograms in figures 13 and 14 are the relatively strong negative velocity components (notice that the red features extend below zero velocity). Since the only body parts that move with negative velocity in our model are the arms (as we

already established in section 3.2), we conclude that the arms contribution to the spectrogram is much stronger than at straight-on incidence. The negative velocity features observed in figures 13 and 14 are the result of the arms backscattering becoming dominant at the same time with the fastest backward arm motion.

The overall conclusion is that, if the walking direction forms a large azimuth angle with the radar's line of sight, we cannot expect to detect the regular zigzag pattern that we evidenced in the spectrogram in figure 3.

3.6 Radar Mounted on Airborne Platforms

In this section we consider the case where the radar is mounted on an airborne platform (in the previous sections, the radar was assumed to be ground based). The main modification is the fact that the elevation angle (as measured from the *x*-*y* plane) becomes positive. Also, we add an infinite ground plane with dielectric constant $\varepsilon_r = 10$ and conductivity $\sigma = 0.005$ S/m (these correspond to relatively wet soil). For this scenario it is interesting to examine both V-V and horizontal-horizontal (H-H) polarizations. The elevation angle is $\theta = 30°$ and all the other radar parameters are kept the same as in section 3.1. The spectrograms are presented in figures 16 (for $\phi = 0°$) and 17 (for $\phi = 60°$).

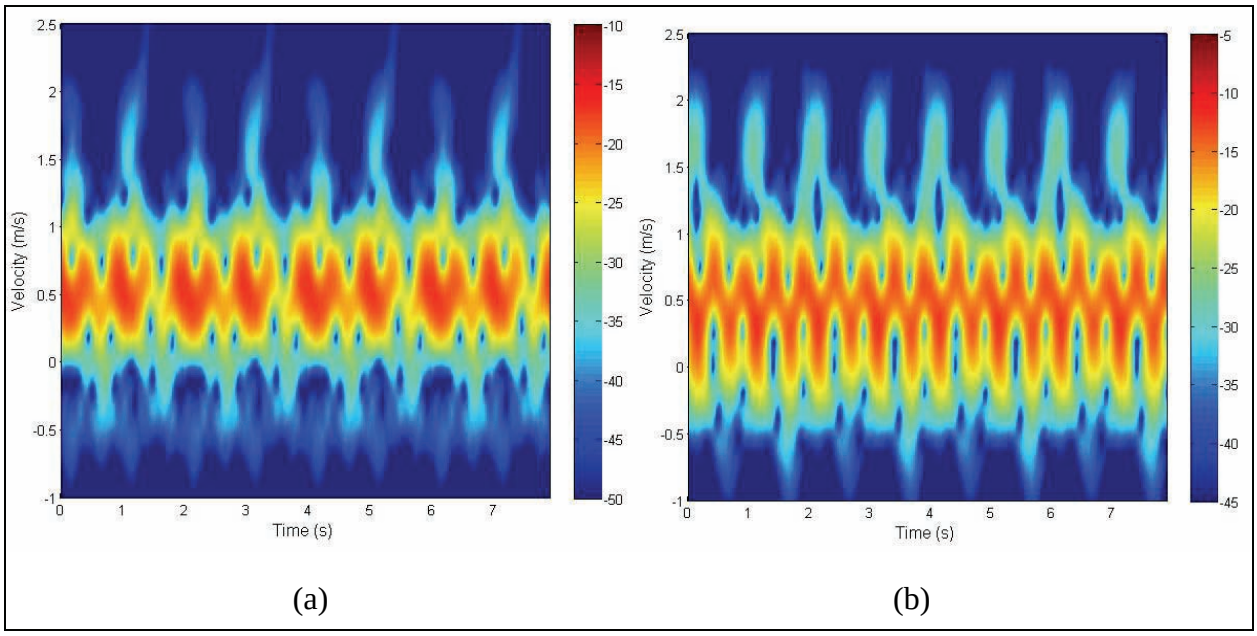

Figure 16. Spectrogram of the full human body in walking motion at 1 GHz, for 30° elevation and 0° azimuth incidence angles, showing (a) V-V polarization and (b) H-H polarization.

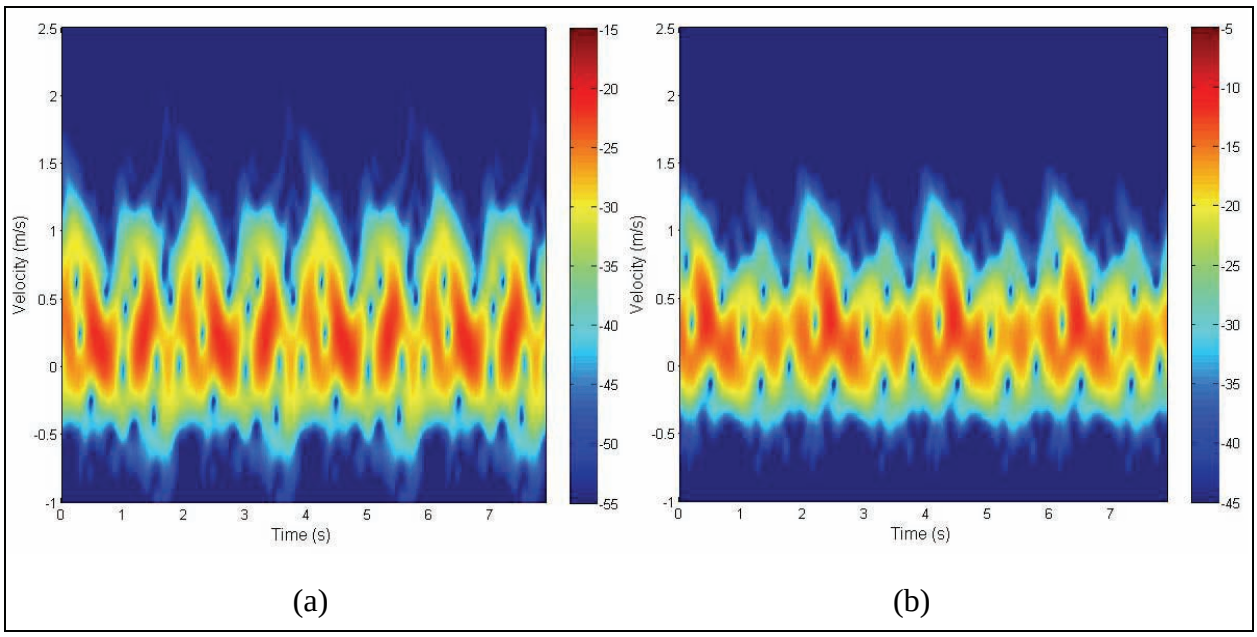

Figure 17. Spectrogram of the full human body in walking motion at 1 GHz, for 30° elevation and 60° azimuth incidence angles, showing (a) V-V polarization and (b) H-H polarization.

Since the incidence angle (in elevation) is close to the Brewster angle (*15*) (which in this case equals $\theta = 22°$), the ground bounce is very weak for V-V polarization and the overall signature is stronger in H-H polarization (notice that the decibels scales have different magnitudes for the two polarizations). The radar return for V-V polarization is mainly produced by the direct scattering from the body. Notice in figure 16a that the pattern changes (compared to figure 3), since now, there are positions of the arms and legs that produce significant backscatter return as compared to the torso (namely, when the legs and arms are perpendicular to the direction of incidence). However, in figure 16b we see the same regular zigzag pattern as in figure 3, which indicates that, in this case (H-H polarization), the torso is again the dominant backscatter contributor, through the corner effect mechanism of the double ground-torso bounce.

When we look at oblique incidence in both elevation and azimuth (as in figure 17), the zigzag pattern is lost in both polarizations, showing that the torso return becomes less important. In fact, the strong negative velocity components in the spectrograms in figure 17 suggest again that the arms have a significant contribution, similar to section 3.5.

3.7 Spectrograms in the UHF band (300 MHz)

Another case where we noticed a change in the scattering phenomenology, as well as in the qualitative aspect of the spectrograms, is that of the radar operating at lower frequencies, in the ultra-high frequency (UHF) band. This frequency range is more characteristic to FOPEN radar systems. In figures 18 through 20 we consider a center frequency of 300 MHz and a bandwidth of 40 MHz. All the other parameters are the same as in section 3.1 and both the azimuth and elevation angles are 00. In figure 18 we show the spectrogram obtained for the full human body

mesh in walking motion. Notice that, qualitatively, this looks very different from the spectrogram in figure 3.

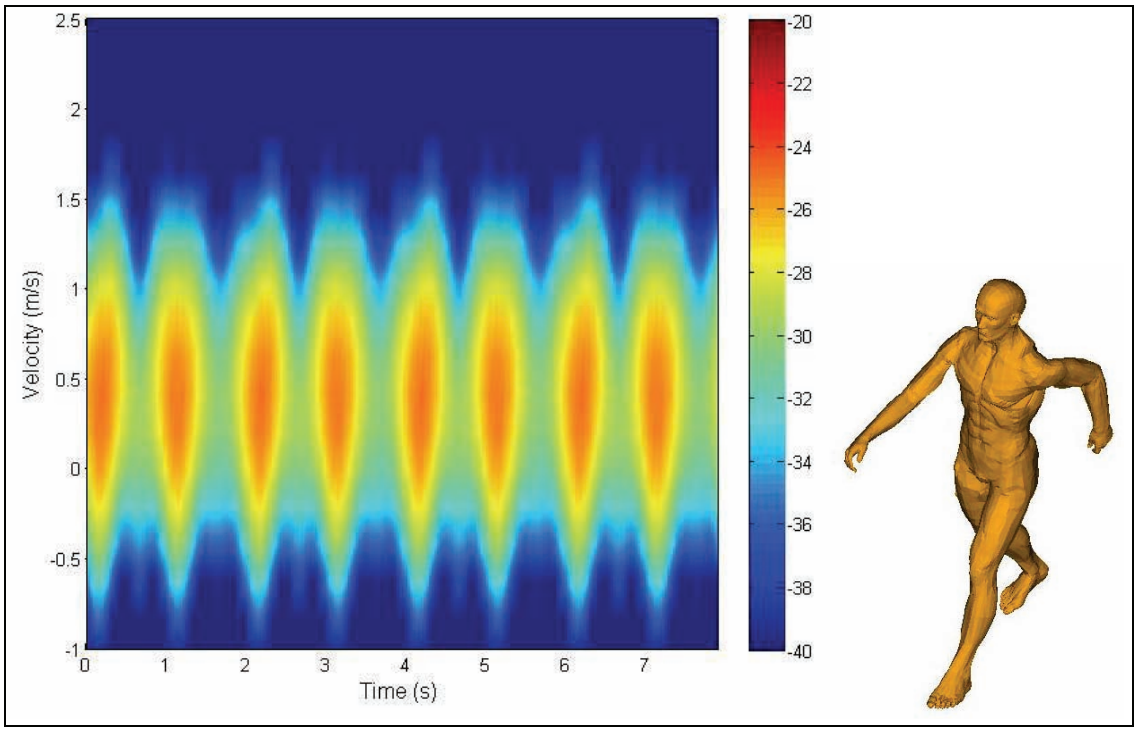

Figure 18. Spectrogram of the full human body in walking motion (directly towards the radar) at 300 MHz.

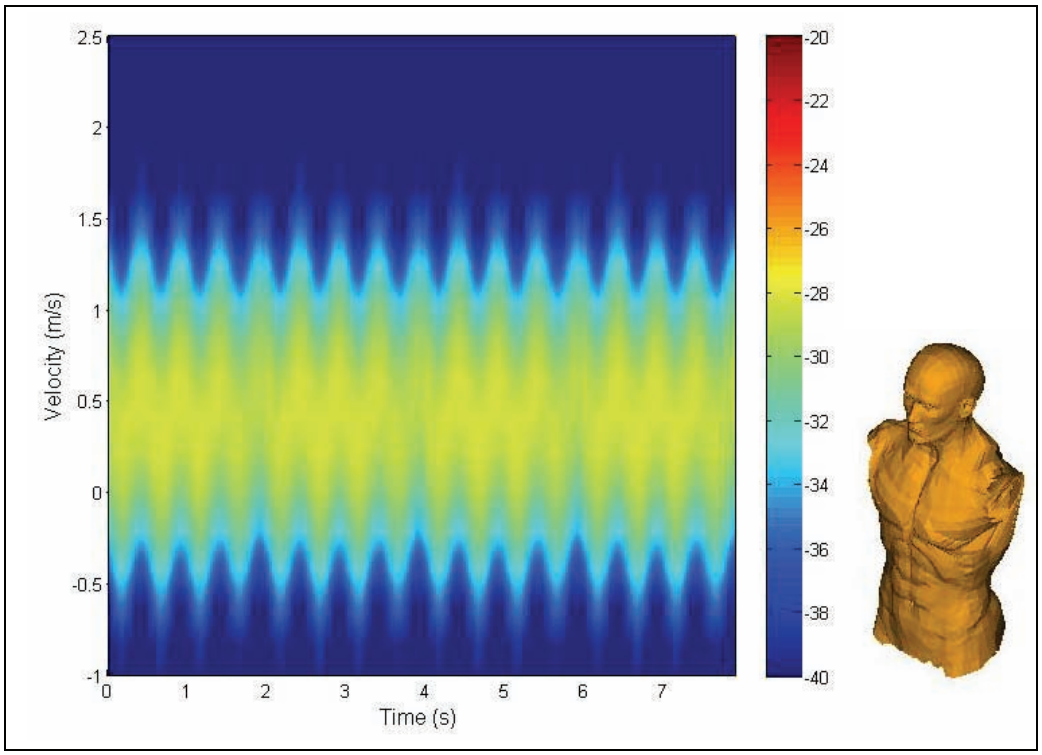

Figure 19. Spectrogram of the torso and head contribution to the Doppler signature at 300 MHz.

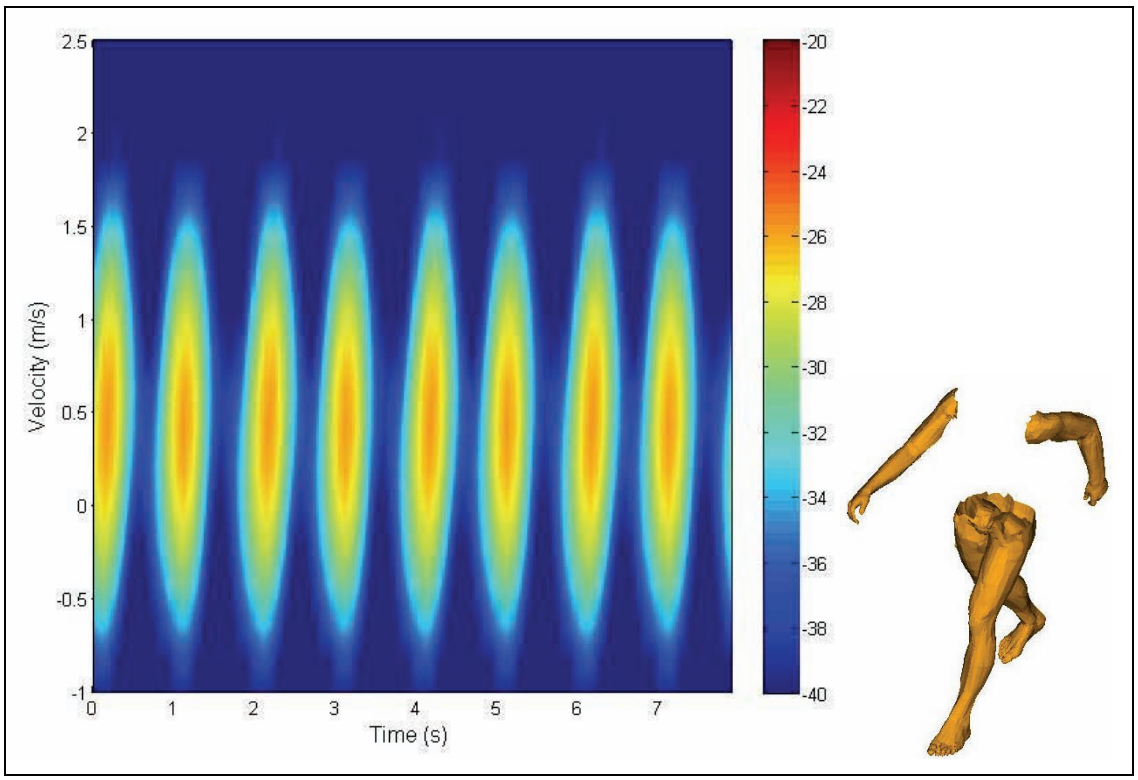

Figure 20. Spectrogram of the arms and legs contribution to the Doppler signature at 300 MHz.

A more careful analysis demonstrates that the pattern in figure 18 is produced by the arms and the legs creating a larger backscattering return than the torso in certain body positions during the walking cycle, at these low frequencies. Thus, in figure 19 we notice that the torso alone produces the same regular zigzag pattern as in figure 3. However, its contribution is overshadowed by the arms and legs contribution, shown in figure 20. Similar to the analysis in section 3.2, we plot the RCS of various body components as a function of the frame number in figure 21.

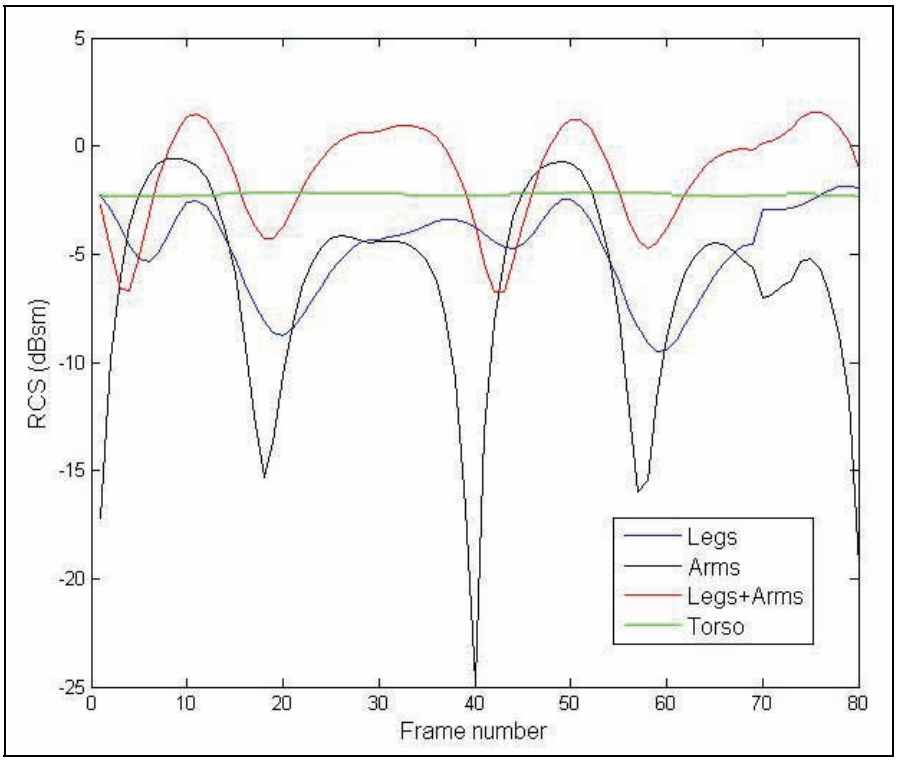

Figure 21. Frame-by-frame contribution of different body parts to the radar cross section at 300 MHz.

This time we notice that, when taken separately, the arms have larger RCS than the legs. Also, there are two distinct peaks of the arms RCS that exceed the torso contribution. However, when we put together the arms and legs, we obtain an overall RCS that is significantly higher than the parts taken separately. This is indicative of the fact that there is strong coupling between body parts at these low frequencies (where the wavelength is on the order of 1 m). At times, the arms plus legs RCS exceeds the torso RCS by about 4–5 dB, which explains why the spectrogram in figure 20 displays significantly higher peaks than the one in figure 19. Moreover, in figure 22 we notice that the full body RCS clearly exceed the peaks produced by the body parts separately, demonstrating that there is a strong overall coupling between legs, arms and torso in this frequency range. This is consistent with the spectrogram in figure 18, which has intensity peaks of about 6–7 dB above the intensity peaks in figure 19.

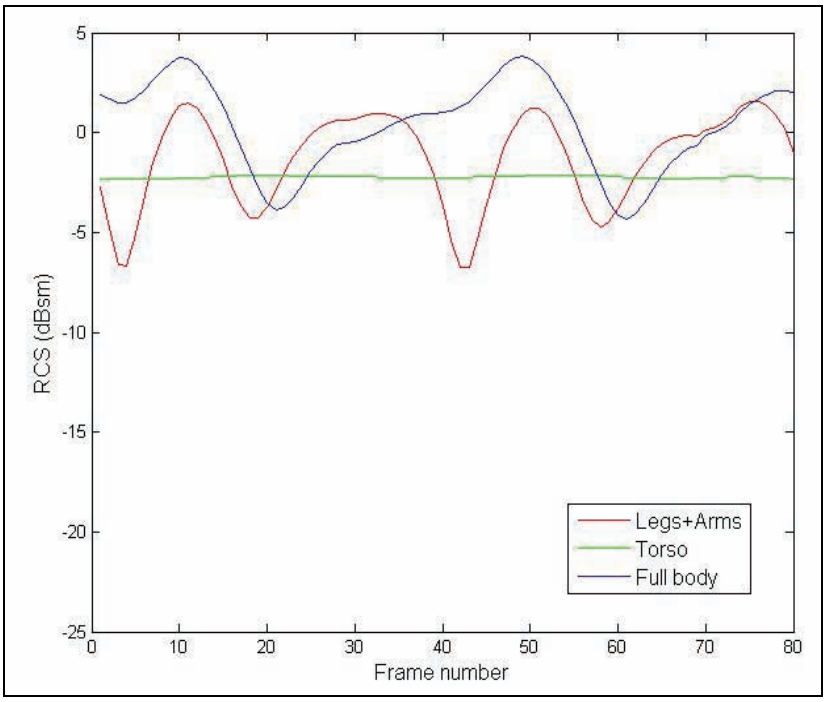

Figure 22. Frame-by-frame comparison of the full body RCS with the contribution of different body parts at 300 MHz.

Similar to the spectrograms presented in the previous two sections, when the arms create significant backscatter contribution, we notice some strong negative velocity components (in both figures 18 and 20). As we already mentioned in section 3.2, this effect is specific to our computer animation models and may not necessarily reflect the true motion of the arms for natural human walking. Nevertheless, this case represents yet another illustration where a change in the scattering phenomenology may require a different way of interpreting the temporal variations in the Doppler spectrum.

4. Conclusions

In previous work (*1*), we concluded that the human body has a fairly large radar signature, which can be detected through many types of obstacles. However, the major issue is being able to discriminate a human body signature from that of other objects present in a scene. At the current stage of our work, it is difficult to identify salient features of a stationary human that provide enough information to an automatic target recognition engine searching for the human presence in such an environment. Most likely, a through-the-wall or through-vegetation human body detection scheme must rely on analyzing the Doppler signature of the human motion. Moreover, the time variations of the human Doppler spectrum need to be investigated in order to discriminate humans from other movers or classify targets of interest based on certain biometric features.

In this report we performed a time-frequency analysis of the Doppler signature of a walking human, based on computer models. The emphasis was on explaining the patterns in the Doppler spectrograms from an EM phenomenological point of view. This is important in understanding the relative contribution of various body parts, as well as the influence of certain radar or geometric parameters. We showed that, at frequencies around a 1 GHz, when the human walks straight to the radar, a regular zigzag pattern is obtained, with the main contribution from the human torso. The middle of the zigzag pattern closely follows the velocity of a point on the human's chest, as shown in section 3.1. The spectrogram also exhibits higher velocity "spikes", where most of the contribution comes from the arm motion. We did not notice these "spikes" in the spectrogram of the human carrying an AK47 rifle, since the arms are motionless in that case. This effect suggests an obvious way to discriminate human targets carrying a weapon based on the high-velocity information contained in the Doppler spectrograms.

In general, the spectrograms obtained via simulations at frequencies around 1 GHz reasonably matched radar measurements performed in the Ka-band. However, for large azimuth incidence angles or UHF band frequencies, the spectrograms changed significantly, making the pattern recognition problem more difficult. When the torso produced the dominant radar return among all the body parts, we noticed the well-behaved zigzag pattern evident in section 3.1 through 3.4. On the other hand, when other body parts became the dominant scatterers, or there was strong coupling between various body parts (such as in sections 3.5 through 3.7), we saw different spectrogram patterns, dictated by the new scattering phenomenology. This clearly illustrates the importance of understanding the EM phenomenology before we try to interpret the spectrograms via signal processing algorithms.

One persistent question about our analysis concerns how closely the motion of the human meshes in our simulations matches a real life scenario. As future work, we plan to incorporate motion data that comes directly from measurements of live human subjects. This would increase our level of confidence in the Doppler spectrograms obtained as a result of applying high fidelity EM modeling to realistic meshes. Ultimately, it is the comparison with experimental radar data that would validate our computer simulations. It would also be interesting to investigate other type of human motions, such as running, crawling, swaying, or even breathing. Another scenario that requires attention is that of a human moving inside a room, where multipath propagation may create complications in the Doppler spectrogram patterns.

It was not the purpose of our study to tackle the problems of feature extraction and pattern recognition that would ultimately discriminate between humans and other movers. In order to achieve this, we will need to obtain data (either simulated or measured) on the Doppler signature of other movers, such as animals. Then, we will need to apply advanced signal processing techniques in order to interpret the radar data and classify the type of movers based on their Doppler signatures. As demonstrated by our analysis, this may prove particularly challenging for certain geometries or radar frequencies.

5. References

1. Dogaru, T.; Nguyen, L.; Le, C. *Computer Models of the Human Body Signature for Sensing Through the Wall Radar Applications*; ARL-TR-4290; U.S. Army Research Laboratory: Adelphi, MD, September 2007.
2. Le, C.; Dogaru, T. *Numerical Modeling of the Airborne Radar Signature of Dismount Personnel in the UHF-, L-, Ku- and Ka-Bands*; ARL-TR-4336; U.S. Army Research Laboratory: Adelphi, MD, December 2008.
3. Dogaru, T.; Le, C. *Validation of Xpatch Computer Models for Human Body Radar Signature*; ARL-TR-4403; U.S. Army Research Laboratory: Adelphi, MD, March 2008.
4. Antony, R. *Target classification for the installation security radar system*; HDL-TR-1976, Harry Diamond Laboratories, November 1981.
5. Van Dorp, P.; Groen, F.C.A. Radar human walking estimation with radar, sonar and navigation. *IEE Proceedings* **October 2003**, *150*, 356–365.
6. Geisheimer, J. L.; Marshall, W. S.; Greneker, E. A continuous-wave (CW) radar for gait analysis. *Record of the 35th Asilomar Conference on Systems and Computers* **November 2001**, *1*, 834–838.
7. Lin, A.; Ling, H. Frontal imaging of human using three-element Doppler and direction-of-arrival radar. *Electronics Letters* **May 2006**, *42*, 660–661.
8. Lai, C.-P.; Ruan, Q.; Narayanan, R. M. Hilbert-Huang Transform (HHT) analysis of human activities using through-wall noise radar. *2007 International Symposium on Signals, Systems and Electronics* **July 2007**, 115–118.
9. Skolnik M. *Introduction to Radar Systems*, McGraw-Hill, New York, 2001.
10. Autodesk Web page. http://www.autodesk.com/maya (accessed June 2007).
11. Taflove, A.; Hagness, S. C. *Computational Electrodynamics: The Finite-Difference Time-Domain*, Artech House, Boston, MA, 2000.
12. Kunz, K.; Luebbers, R. *The Finite-Difference Time-Domain Method for Electromagnetics*, CRC Press, Boca Raton, FL, 1993.
13. Oppenheim, A. V.; Schafer, R. W. *Discrete-Time Signal Processing*, Prentice Hall, Englewood Cliffs, NJ, 1989.
14. ARL MSRC Web page. http://www.arl.hpc.mil (accessed August 2007).
15. Balanis, C. *Advanced Engineering Electromagnetics*, Wiley, New York, 1989.

Acronyms

ARL	U.S. Army Research Laboratory
CAD	computer-aided design
CEM	computational electromagnetics
CERDEC	Communications-Electronics Research Development and Engineering Center
CPI	coherent processing interval
EM	electromagnetic
FDTD	Finite Difference Time Domain
FOPEN	foliage penetration
H-H	horizontal-horizontal
HPC	High-Performance Computing
I2WD	Intelligence and Information Warfare Directorate
I-Q	in-phase-quadrature
MSRC	Major Shared Resource Center
ONR	Office of Naval Research
PC	personal computer
PEC	perfect electric conductor
PRF	pulse repetition frequency
RCS	radar cross section
RF	radio frequency
STFT	Short-Time Fourier Transform
STTW	sensing through the wall
UHF	ultra-high frequencies
UWB	ultra-wideband
V-V	vertical-vertical

No. of Copies	Organization
1	ADMNSTR
PDF	DEFNS TECHL INFO CTR ATTN DTIC OCP 8725 JOHN J KINGMAN RD STE 0944 FT BELVOIR VA 22060-6218
1	DARPA ATTN IXO S WELBY 3701 N FAIRFAX DR ARLINGTON VA 22203-1714
1 CD	OFC OF THE SECY OF DEFNS ATTN ODDRE (R&AT) THE PENTAGON WASHINGTON DC 20301-3080
1	US ARMY RSRCH DEV & ENGRG CMND ARMAMENT RSRCH DEV & ENGRG CTR ARMAMENT ENGRG & TECHNLGY CTR ATTN AMSRD AAR AEF T J MATTS BLDG 305 APG MD 21005-500
2	US ARMY RDECOM CERDEC I2WD ATTN AMSRD CER IW IM W CHIN BLDG 600 MCAFEE CENTER FT MONMOUTH NJ 07703
1	PM TIMS PROFILER (MMS P) AN/TMQ 52 ATTN B GRIFFIES BUILDING 563 FT MONMOUTH NJ 07703
1	US ARMY RDECOM CERDEC I2WD ATTN AMSRD-CER-IW-RA V FEDOROW BLDG 600 MCAFEE CTR FT MONMOUTH NJ 07703
1	US NAVAL RSRCH LAB RADAR DIV ADAPTIVE PROCESSING SECTION ATTN A DESROSIERS 4555 OVERLOOK AVE SW WASHINGTON DC 20375-5312
1	SMC/GPA 2420 VELA WAY STE 1866 EL SEGUNDO CA 90245-4659

No. of Copies	Organization
1	US ARMY INFO SYS ENGRG CMND ATTN AMSEL IE TD F JENIA FT HUACHUCA AZ 85613-5300
1	COMMANDER US ARMY RDECOM ATTN AMSRD AMR W C MCCORKLE 5400 FOWLER RD REDSTONE ARSENAL AL 35898-5000
1	US ARMY RSRCH LAB ATTN AMSRD ARL CI OK TP TECHL LIB T LANDFRIED BLDG 4600 APG MD 21005-5066
1	US GOVERNMENT PRINT OFF DEPOSITORY RECEIVING SECTION ATTN MAIL STOP IDAD J TATE 732 NORTH CAPITOL ST NW WASHINGTON DC 20402
1	DIRECTOR US ARMY RSRCH LAB ATTN AMSRD ARL RO EV W D BACH PO BOX 12211 RESEARCH TRIANGLE PARK NC 27709
15	US ARMY RSRCH LAB ATTN AMSRD ARL CI OK T TECHL PUB ATTN AMSRD ARL CI OK TL TECHL LIB ATTN AMSRD ARL SE RU A SULLIVAN ATTN AMSRD ARL SE RU C LE ATTN AMSRD ARL SE RU G KIROSE ATTN AMSRD ARL SE RU K KAPPRA ATTN AMSRD ARL SE RM J SILVIOUS ATTN AMSRD ARL SE RM D WIKNER ATTN AMSRD ARL SE RM D TAHMOUSH ATTN AMSRD ARL SE RM T PIZZILLO ATTN AMSRD ARL SE RU K RANNEY ATTN AMSRD ARL SE RU A MARTONE ATTN AMSRD ARL SE RU T DOGARU (2 COPIES) ATTN IMNE ALC HR MAIL & RECORDS MGMT ADELPHI MD 20783-1197

TOTAL: 30 (1 elec, 28 HCs, 1 CD)